1-1-2014

Device for detailed analysis of leakage current paths in photovoltaic modules under high voltage bias

Neelkanth G. Dhere
University of Central Florida

Narendra S. Shiradkar
University of Central Florida

Eric Schneller
University of Central Florida

Device for detailed analysis of leakage current paths in photovoltaic modules under high voltage bias

Cite as: Appl. Phys. Lett. **104**, 112103 (2014); https://doi.org/10.1063/1.4869028
Submitted: 13 December 2013 . Accepted: 07 March 2014 . Published Online: 18 March 2014

Neelkanth G. Dhere, Narendra S. Shiradkar, and Eric Schneller

APPLIED PHYSICS LETTERS **104**, 112103 (2014)

Device for detailed analysis of leakage current paths in photovoltaic modules under high voltage bias

Neelkanth G. Dhere,[a)] Narendra S. Shiradkar, and Eric Schneller
Florida Solar Energy Center, University of Central Florida, 1679 Clearlake Road, Cocoa, Florida 32922, USA

(Received 13 December 2013; accepted 7 March 2014; published online 18 March 2014)

High voltages used in photovoltaic (PV) systems are known to induce long-term power loss in PV modules due to leakage current flowing through the module packaging materials. It has been difficult to identify the specific materials and interfaces responsible for degradation based on an analysis of only the total leakage current. A detailed investigation of the leakage current paths within the PV modules, under high voltage bias, is carried out by utilizing a device that measures the independent contributions of various paths in real-time. Knowledge about dominant leakage current paths can be used to quantify the physical and chemical changes occurring within the module packaging materials. © *2014 AIP Publishing LLC*. [http://dx.doi.org/10.1063/1.4869028]

In order for energy from photovoltaic (PV) systems to remain cost-competitive with traditional sources, the long-term reliability of PV modules must be assured.[1–4] To achieve this, key failure modes must be identified and their occurrence suppressed in a cost-effective manner. PV systems consist of one or more module strings, made up of several modules connected in series, to reduce the balance of system costs.[5] This arrangement leads to high system voltages that can reach up to 1000 V. Safety requirements ensure that all exposed metal surfaces, including the module frame, are properly grounded.[6,7] Some modules experience very high potential differences between the cell circuit and the module frame due to this requirement. Degradation arising from system voltage stress has been identified as a significant long-term failure mode in PV modules, known as Potential Induced Degradation (PID) or System Voltage Induced Degradation (SVID).[8,9] This potential difference results in a leakage current that flows through the packaging materials of the module that includes structural materials such as the front glass, encapsulant, and backsheet.

The magnitude of this leakage current has been considered as an approximate indicator of the susceptibility of a PV module to PID.[10–12] The Florida Solar Energy Center (FSEC) has pioneered the study of PV modules under high voltage bias in the hot and humid climate.[5] Conditions of high temperature and relative humidity have been identified to accelerate the degradation resulting from system voltage stress.[6] Attempts have been made to analyze the relationship between the total measured leakage current and the resulting performance loss over the past 13 yr.[10–12] The correlation of the physical and chemical changes of the module materials with the system voltage, meteorological parameters, and total leakage current has been difficult due to the complex nature of the leakage current in the PV modules.[13–17] Fig. 1(a) shows the various leakage current pathways in a PV module. It has been difficult to identify the specific pathway(s) responsible for materials degradation within the module because the magnitude of the total leakage current is a parallel combination of leakage current flowing through these pathways. Based on the need to elucidate this degradation mode, a device (custom laminate) was developed to allow physical measurement of the leakage current flowing through these individual pathways in real-time. This provides electrical signatures of the changes occurring at the surfaces, internal interfaces, and the bulk of the module's packaging materials. Figs. 1(b) and 1(c) show the top and cross-sectional views of the custom laminate, respectively (patent pending).[18]

At FSEC, several commercial multicrystalline silicon PV modules were deployed on an outdoor test bed with an applied voltage bias of −600 V with respect to ground. Measurements of the leakage current flowing through the module packaging materials, along with all relevant meteorological parameters, were recorded every minute. The module packaging materials consisted of sodalime glass as the front cover, ethylene-vinyl-acetate (EVA) as the encapsulant, and tedlar-polyester-tedlar (TPT) as the backsheet. The custom laminate—consisting of front glass, encapsulant, and backsheet laminated together with strategically placed electrodes was also deployed alongside the modules to measure leakage currents flowing through the glass-EVA and TPT-EVA interfaces, bulk EVA, and the glass surface in the custom laminate. Meteorological parameters such as ambient temperature, back of module temperature, solar irradiance, relative humidity, dew point temperature, and surface wetness were also measured in real-time.

Equations (1) and (2) are used to calculate the bulk resistivity of EVA and the sheet resistance of interfaces, respectively, from the custom laminate

$$\rho_{EVA} = \frac{V}{I_L} \times \frac{A_{cross}}{t_{EVA}}, \tag{1}$$

$$R_{sheet,i} = \frac{V}{I_L} \times N_{laminate}, \tag{2}$$

where ρ_{EVA} is bulk resistivity of EVA, V is applied voltage, I_L is corresponding leakage current, A_{cross} is cross sectional area of electrodes in custom laminate, t_{EVA} is thickness of

a)Author to whom correspondence should be addressed. Electronic mail: dhere@fsec.ucf.edu

EVA, R_{sheet} is sheet resistance of interface "i", and $N_{laminate}$ is the number of squares in parallel in the custom laminate. The following values were used for the parameters in Eqs. (1) and (2) in this study: $V = -600\,V$, $A_{cross} = 25 \times 10^{-6}\,m^2$, $t_{EVA} = 5 \times 10^{-4}$ m, and $N_{laminate} = 37$. The values of ρ_{EVA} and R_{sheet} of glass-EVA and TPT-EVA interfaces as a function of time calculated from Eqs. (1) and (2) are used to calculate the instantaneous leakage current for a 60-cell commercial PV module using Eqs. (3)–(10). Earlier, it has been shown that when the module is dry, the leakage current mainly flows in the sideways direction to the frame of the module through parallel paths 1, 2, 3, and 4.[19] The bulk resistivity of the TPT backsheet is several orders of magnitude higher than that of other materials, and hence its contribution can be neglected. The following equations describe the procedure used to calculate the module leakage current using the values of bulk resistivity of EVA and the sheet resistances of the various interfaces obtained from Eqs. (1) and (2)

$$I_{Module,Dry} = \frac{V}{R_1} + \frac{V}{R_2} + \frac{V}{R_3} + \frac{V}{R_4}, \tag{3}$$

$$R_1 = \rho_{EVA} \times \frac{t_{EVA}}{2(L+W) \times U_{EVA}} + \rho_{glass} \times \frac{S}{2(L+W) \times t_{glass}}, \tag{4}$$

$$R_2 = \rho_{EVA} \times \frac{t_{EVA}}{2(L+W) \times U_{EVA}} + \frac{R_{Sheet,Glass-EVA}}{N_{module}}, \tag{5}$$

$$R_3 = \rho_{EVA} \times \frac{S}{2(L+W) \times 2t_{EVA}}, \tag{6}$$

$$R_4 = \rho_{EVA} \times \frac{t_{EVA}}{2(L+W) \times U_{EVA}} + \frac{R_{Sheet,TPT-EVA}}{N_{module}}, \tag{7}$$

where R_i is the resistance of the corresponding path, L and W are the length and width of the module, t_{EVA} and t_{glass} are the thicknesses of EVA and the glass, S is the sideways distance from the edge of the cell to the frame, and N_{module} is the number of squares in the PV module for the purpose of effective sheet resistance calculations. The parameter U_{EVA} is the effective length of the EVA strip between the edge of the cell and a point in the interior of the cell from which the current can be assumed to flow upward and is estimated from the finite element analysis simulations.[18] The following parameters values are used in this study: $L = 1.65\,m$, $W = 1\,m$, $S = 0.02\,m$, $\rho_{glass} = 5 \times 10^{10}\,\Omega$-m, $U_{EVA} = 0.005\,m$, and $t_{glass} = 0.0032\,m$. The parameter N_{module} is calculated to be 265 from

$$N_{module} = \frac{2 \times (L+W)}{S}. \tag{8}$$

The values of ρ_{EVA} and R_{sheet} of the glass-EVA and TPT-EVA interfaces are determined from the measured values of leakage currents every minute. The overall leakage current for a 60-cell module is calculated from each of the separate components and is compared with the observed values of leakage current for commercial modules during a 3-h interval on a typical dry afternoon. The calculated and observed leakage currents follow similar trends with time as shown in Fig. 2(a). The absolute value of the leakage current calculated from the laminate is somewhat higher than the measured values. This can be attributed to inherent differences in the packaging materials (e.g., encapsulant formulations) or the processing parameters (e.g., lamination time and temperature) used in the construction of the laminate and the module. However, the dominant leakage current paths predicted by the laminate and those observed in the actual module are expected to be similar due to similar packaging schemes.

Fig. 2(b) shows a Pie chart of averaged values of leakage current from all four paths in this time interval. It is apparent that the interfaces constitute the dominant leakage current paths in this particular case. The glass plays an important role in determining the leakage current through the paths 1 and 2. The encapsulant plays an important role in determining the leakage current through all paths. The large contribution of leakage current observed from path 4 can be explained as follows: Due to difficulties in adhesion to the

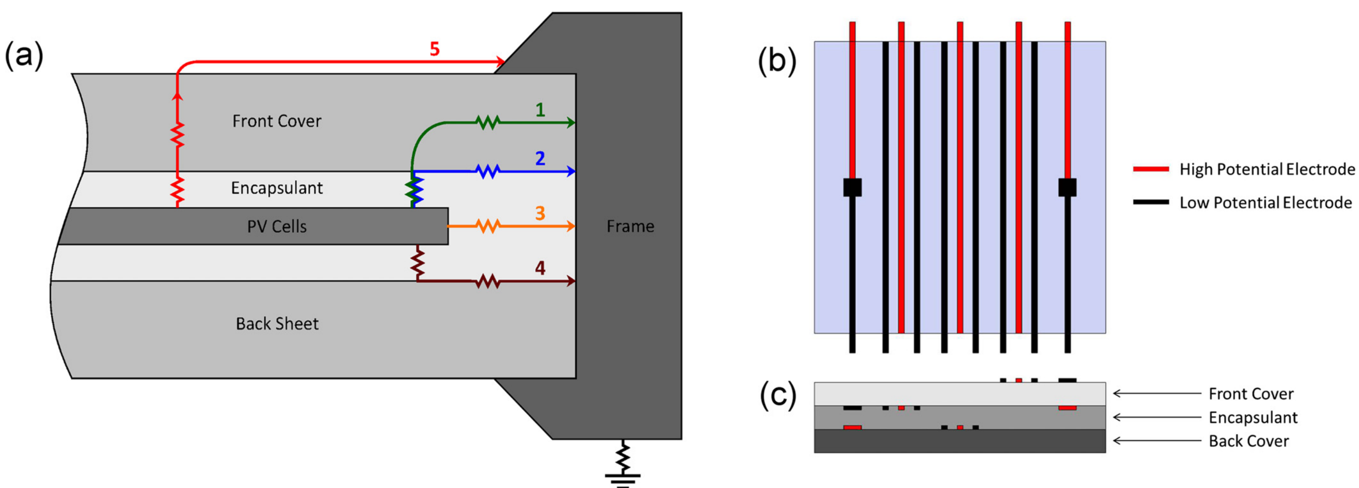

FIG. 1. (a) Cross section of a PV module depicting the leakage current paths. When the module is dry the current flows through paths 1–4, due to a sideways oriented electric field. The relative distribution among these paths is determined by the resistivity of materials and sheet resistances of interfaces. When the module is wet, the leakage current predominantly flows through path 5 due to a vertically oriented electric field along the whole module and the low resistance of path 5 owing to a wet surface that is grounded. (b) Top and (c) cross-sectional views of the custom laminate. The leakage current flowing through the high and low potential electrodes is measured in real-time to calculate bulk resistivity of EVA, glass, and sheet resistance of the interfaces.

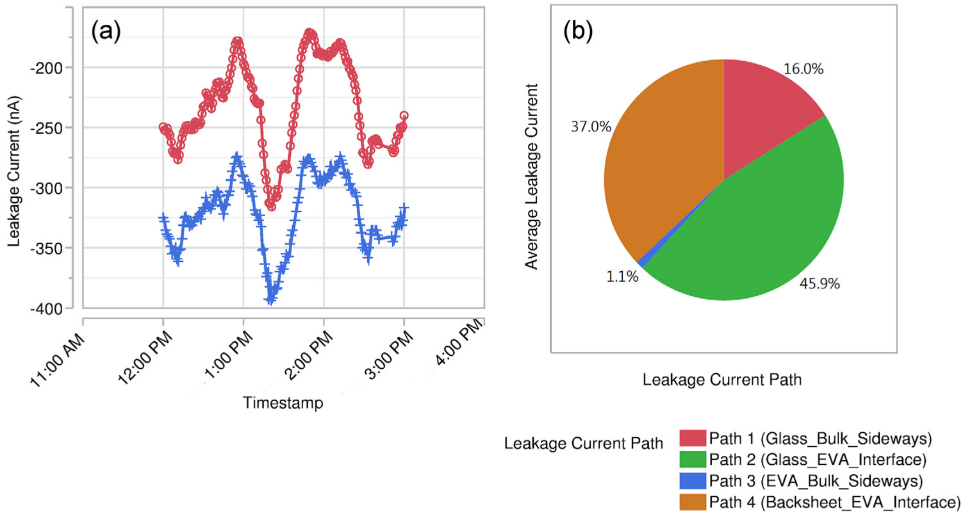

FIG. 2. (a) Observed leakage current of a 60-cell commercial module and calculated leakage current from the laminate show similar trends. (b) Pie-chart of the averaged values of leakage currents through paths 1–4 in this time interval. Glass plays an important role in determining the majority of the leakage current (Path 1 + Path 2).

TPT backsheet, the metallic ribbons were physically compressed against the backsheet during lamination process. Some amount of EVA can get trapped below the ribbons. Due to significantly lower resistivity of EVA as compared to that of TPT, the trapped EVA can reduce the effective sheet resistance, thereby increasing the leakage current.

When the module front glass is wet, resulting from condensation or rain, it has been shown that paths 1–5 are in parallel and the majority of leakage current flows through path 5, due to its lower resistance. The following equations can be used to calculate the module leakage current in dry, wet, and intermediate conditions

$$I_{module} = I_{module,dry} + w \times I_{module,wet}, \tag{9}$$

$$I_{module,wet} = \frac{V}{\left(\rho_{EVA \times \frac{t_{EVA}}{L \times W}}\right) + \left(\rho_{glass \times \frac{t_{glass}}{L \times W}}\right)}, \tag{10}$$

where w is the percentage of surface wetness measured by the wetness sensor, the value of parameter w is 0% when the surface is dry, while it is 100% when the surface is completely wet. The value of $I_{Module,Dry}$ is taken from Eq. (3), thus in perfectly dry conditions, Eq. (9) reduces to Eq. (3), while in completely wet conditions, Eq. (9) reduces to Eq. (10). In order to validate the equations, a time interval from 9:00 PM to 6:00 AM was chosen, during which the wetness values vary from 0% to 100%. Fig. 3 shows that during this interval, the relative humidity is consistently between 90% and 95%, while the ambient and back-of-the-module temperatures remain between 20 and 25 °C. The wetness is close to zero at the beginning and it is seen to undergo a steep transition to 100% around midnight due to condensation. This finding is consistent with the earlier reported results describing orders of magnitude higher current during an event of rain or early morning condensation.[20] Fig. 3 also shows the typical observed leakage current from a commercial 60-cell module and leakage current calculated from the laminate using Eq. (9). The leakage current increases steeply as the wetness increases from 0% to 100%. Once the condensate on the front glass of the module provides a continuous path, the leakage current stabilizes to a consistently high value. The observed leakage current from a module and the leakage current calculated from laminate follow a similar trend. The differences in the absolute values of leakage current are, again, artifacts of the differences in the materials used for the construction of laminate and the module.

Calculation of activation energies has been reported for various relative humidity ranges for modules undergoing outdoor high voltage bias testing by applying the Arrhenius relationship between the total leakage current, relative humidity, and back of the module temperature.[11,20] However, this approach can only yield activation energy corresponding to the dominant leakage current pathway. By using the custom laminate in a similar study, it is possible to calculate the activation energies for each leakage current pathway and understand the underlying physics for individual leakage current paths.

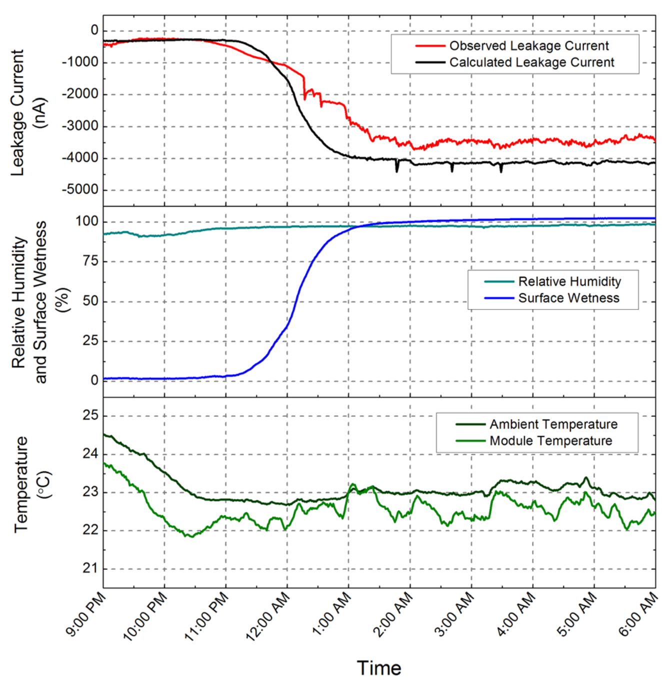

FIG. 3. Meteorological parameters during the time interval from 9 PM to 6 AM. Surface wetness is seen to increase from 0% to 100% due to condensation. Observed and calculated values of leakage current show a similar trend, increasing by an order of magnitude after the condensation.

In summary, it has been difficult to identify the specific materials and interfaces responsible for the degradation of commercial PV modules, under high voltage bias, based only on the analysis of total leakage current. Now with the development of a custom laminate, however, the independent contributions of various leakage current paths can be determined. The custom laminate is used to measure the values of bulk resistivity of EVA and the sheet resistances of the interfaces in real-time. These values are then used to calculate the total leakage current that would flow in a commercial 60-cell PV module along with the individual contributions from each path. Such analyses can be used to derive correlation of the leakage currents flowing through various paths with the physical and chemical changes occurring in the packaging materials. Now the contribution of each leakage path to the physisorption and chemisorption processes that lead to materials degradation can be quantitatively determined. This cost-effective method of identifying module degradation under high voltage bias will contribute to the long-term reliability of PV modules, thereby keeping them cost-competitive with traditional energy sources.

Authors are thankful to Mr. Vivek Gade, from Jabil Circuit, Inc. for his help in the preparation of the custom laminate.

[1]J. Wohlgemuth and S. Kurtz, in *Proceedings of IEEE International Reliability Physics Symposium*, Monterey, 10 April–14 April (IEEE, 2011), pp. 5E.3.1–5E.3.6.
[2]J. Wohlgemuth, D. W. Cunningham, A. Nguyen, G. Kelly, and D. Amin, in Proceedings of PV Module Reliability Workshop, Golden, USA (Office of Energy Efficiency and Renewable Energy, 2010).
[3]M. D. Kempe, Sol. Energy Mater. Sol. Cells **90**(16), 2720 (2006).
[4]M. Kempe, G. J. Jorgensen, K. M. Terwilliger, T. J. McMahon, C. E. Kennedy, and T. T. Borek, Sol. Energy Mater. Sol. Cells **91**(4), 315 (2007).
[5]N. G. Dhere, in *Proceedings of 31st IEEE Photovoltaic Specialists Conference*, Lake Buena Vista, USA, 03 January–07 January (IEEE, 2005), pp. 1570–1576.
[6]N. G. Dhere, S. Pethe, and A. Kaul, in *Proceedings of PV Module Reliability Workshop*, Golden, USA (Office of Energy Efficiency and Renewable Energy, 2011).
[7]N. G. Dhere, S. Pethe, and A. Kaul, Proc. SPIE **8112**, 81120OR (2011).
[8]P. Hacke, K. Terwilliger, R. Smith, S. Glick, J. Pankow, M. Kempe, S. Kurtz, I. Bennett, and M. Kloos, in *Proceedings of 37th IEEE Photovoltaic Specialists Conference*, Seattle, USA, 19 June–24 June (IEEE, 2011), pp. 19–24.
[9]P. Hacke, R. Smith, K. Terwilliger, S. Glick, D. Jordan, S. Johnston, M. Kempe, and S. Kurtz, IEEE J. Photovolt. **3**(1), 246 (2013).
[10]C. R. Osterwald and T. J. McMahon, Sol. Energy Mater. Sol. Cells **79**, 21 (2003).
[11]J. A. Del Cueto and T. J. McMahon, Prog. Photovolt.: Res. Appl. **10**, 15 (2002).
[12]N. G. Dhere, S. M. Bet, and H. P. Patil, in *Proceedings of World Conference on Photovoltaic Energy Conversion*, Osaka, Japan (IEEE, 2003), pp. 1923–1926.
[13]S. Pingel, O. Frank, M. Winkler, S. Daryan, T. Geipel, H. Hoehne, and J. Berghold. in *Proceedings of 35th IEEE Photovoltaic Specialists Conference*, Honolulu, USA, 20–25 June (IEEE, 2010), pp. 2817–2822.
[14]S. Koch, J. Berghold, D. Nieschalk, C. Seidel, O. Okoroafor, S. Lehmann, and S. Wendlandt, in *Proceedings of PV Module Reliability Workshop,* Golden, USA (Office of Energy Efficiency and Renewable Energy, 2012).
[15]D. Lauscha, V. Naumanna, O. Breitensteinb, J. Bauerb, A. Graffc, J. Bagdahna, and C. Hagendorfa, in *Proceedings of 39th IEEE Photovoltaics Specialists Conference,* Tampa, USA, June 16–June 21 (IEEE, 2013).
[16]S. Koch, J. Berghold, O. Okoroafor, S. Krauter, and P. Grunow, in *Proceedings of 27th European Photovoltaic Conference and Exhibition,* Frankfurt (EUPVSEC, 2012).
[17]M. Koehl and S. Hoffmann, Prog. Photovolt.: Res. Appl. **22**(2), 173 (2012).
[18]N. G. Dhere, R. G. Dhere, N. Shiradkar, and E. Schneller, U.S. patent pending 61/879,871 (19 September, 2013).
[19]N. Shiradkar, E. Schneller, and N. G. Dhere, Proc. SPIE **8825**, 88250G (2013).
[20]N. G. Dhere, N. Shiradkar, and E. Schneller, in *Proceedings of 39th IEEE Photovoltaic Specialists Conference*, Tampa, June 16–June 21 (IEEE, 2013).